BioOne COMPLETE

Piggyback Whorls: A New Theoretical Morphologic Model Reveals Constructional Linkages Among Morphological Characters in Ammonoids

Authors: Ubukata, Takao, Tanabe, Kazushige, Shigeta, Yasunari, Maeda, Haruyoshi, and Mapes, Royal H.

Piggyback whorls: A new theoretical morphologic model reveals constructional linkages among morphological characters in ammonoids

TAKAO UBUKATA, KAZUSHIGE TANABE, YASUNARI SHIGETA, HARUYOSHI MAEDA, and ROYAL H. MAPES

Ubukata, T., Tanabe, K., Shigeta, Y., Maeda, H., and Mapes, R.H. 2008. Piggyback whorls: A new theoretical morphologic model reveals constructional linkages among morphological characters in ammonoids. *Acta Palaeontologica Polonica* 53 (1): 113–128.

A new theoretical morphological model is proposed for the analysis of growth, form and morphospace of ammonoid shells. In this model, the shape of a radial cross section through the shell is simulated by "piggybacking" of successive whorls. The "piggyback whorls model" is defined in terms of the enlarging rate of the perimeter and the proportion of the dorsal wall to the whorl periphery, if an isometric relationship is assumed between perimeter and area of the cross-sectioned whorl. Allometric coefficients on these growth parameters determine how compressed and evolute shells are formed. The present model successfully reproduced some correlations among purely geometric variables that have been reported in previous works and were also observed in our biometric analyses. This model yields a hypothesis of "constructional linkages" between aperture shape and coiling geometry that might provide a functional coupling between hydrostatic and hydrodynamic characters. The model may partly explain Buckman's Law of Covariation between rib features and shell shapes.

Key words: Theoretical morphology, ammonoids, cross-sectional shape, morphospace, constructional linkage, morphological diversity.

Takao Ubukata [sbtubuk@ipc.shizuoka.ac.jp], Institute of Geosciences, Shizuoka University, Oya 836, Surugaku, Shizuoka 422-8529, Japan;
Kazushige Tanabe [tanabe@eps.s.u-tokyo.ac.jp], Department of Earth and Planetary Science, University of Tokyo, Hongo 7-3-1, Bunkyouku, Tokyo 113-0033, Japan;
Yasunari Shigeta [shigeta@kahaku.go.jp], Department of Geology, National Science Museum, Hyakunincho 3-23-1, Shinjukuku, Tokyo 169-0073, Japan;
Haruyoshi Maeda [maeda@kueps.kyoto-u.ac.jp], Department of Geology and Mineralogy, Kyoto University, Kitashirakawa-Oiwakecho, Sakyouku, Kyoto 606-8502, Japan;
Royal H. Mapes [mapes@ohio.edu], Department of Geological Science, Ohio University, Athens, Ohio 45701, USA.

Introduction

Ammonoids have undoubtedly been the most popular targets for morphospace analysis among fossil animals. Since Raup's (1967) pioneer work, large collections of morphological data have been used to explore functional morphology, macroevolutionary trend, and/or disparity of normally coiled ammonoids (Ward 1980; Bayer and McGhee 1984; Saunders and Swan 1984; Swan and Saunders 1987; Nikolaeva and Barskov 1994; Dommergues et al. 1996; Saunders and Work, 1996, 1997; Korn 2000; Korn and Klug 2003; McGowan 2004; Saunders et al. 2004; Gottobrio and Saunders 2005). A theoretical morphological model introduced by Raup (1967) has been widely applied to investigation of ammonoid morphospace, in which gross shell geometries are defined by whorl expansion rate (*W*), width of umbilicus (*D*) and whorl shape (*S*). The occupation patterns of the *W-D-S* morphospace are commonly used for assessing diversity in basic shell geometry. In addition, Saunders and Swan (1984) and Saunders and Work (1996) introduced several different parameters representing sculpture, aperture shape and suture complexity. The Raup's *W*, *D*, *S*, and other metric parameters used previously are suitable for non-destructive morphometric analysis of museum collections, and also available for measurements from photographs in publications. The use of these accessible parameters allows the development of a comprehensive database that includes hundreds of ammonoid taxa. Comparison of these parameters has proven to be a fruitful way for surveying the long-term evolutionary history of morphological diversity of ammonoids (Saunders and Swan 1984; Swan and Saunders 1987; Korn and Klug 2003).

However, previous morphospace analyses were based on data sets collected from adult or submature average individuals and did not deal with ontogenetic change of shell shape, al-
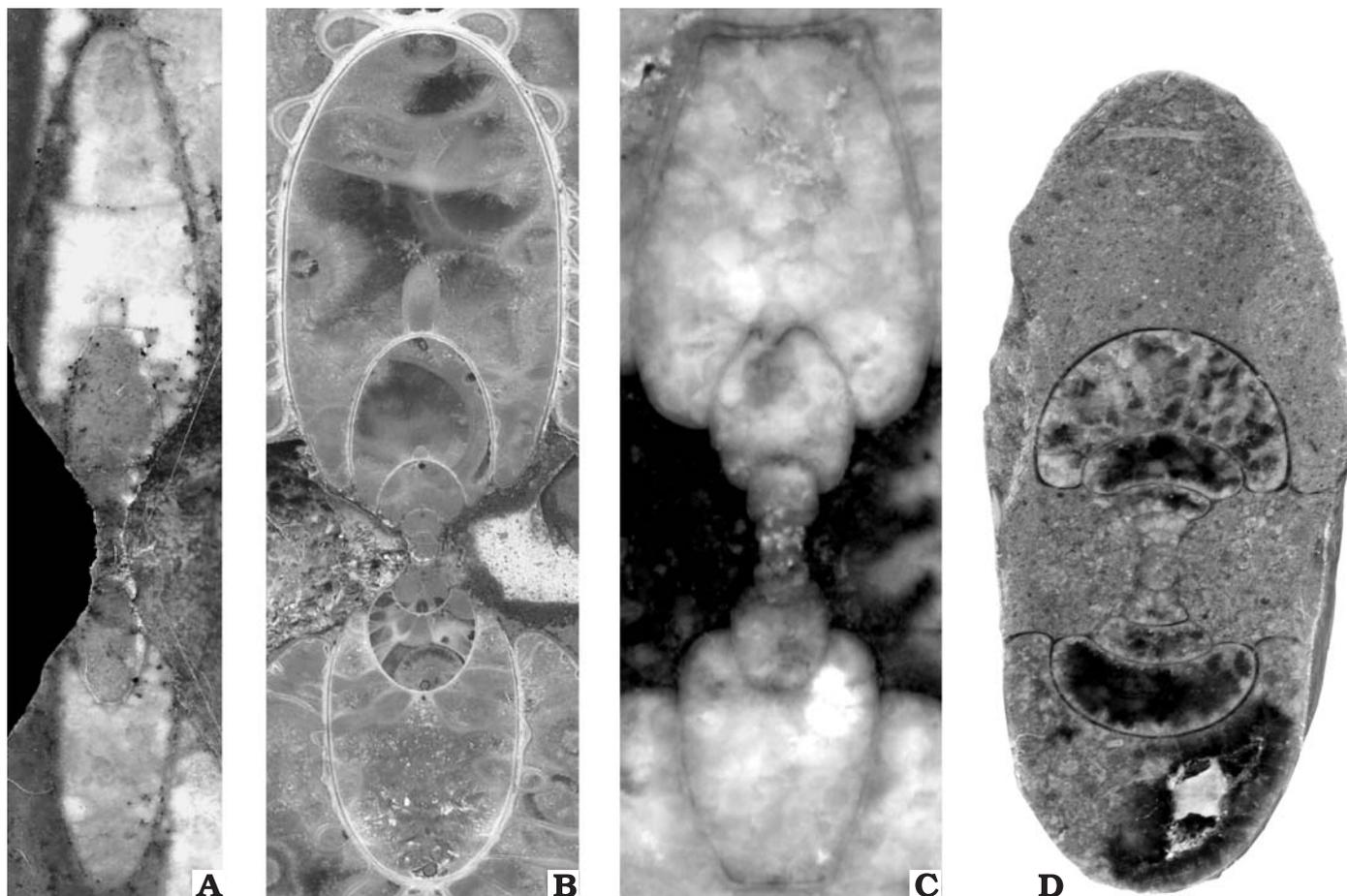
Acta Palaeontol. Pol. 53 (1): 113–128, 2008

http://app.pan.pl/acta53/app53-113.pdf

Fig. 1. Radial cross sections of ammonoids to illustrate allometric growth. **A**. *Beloceras* sp., Devonian; Erfoud, Morocco. **B**. *Phylloceras consanguineum* Gemmellaro, 1876, Jurassic; Sakaraha, Madagascar. **C**. *Meekoceras gracilitatis* White, 1879, Triassic; Crittenden Spring, Nevada. **D**. *Girtyoceras meslerianum* (Girty, 1909), Carboniferous; Jackforth Creek, Oklahoma.

though allometry is common in ammonoids (Fig. 1; e.g., Jacobs 1992; Korn and Klug 2002). Thus, ontogenetic aspects have been incorporated tenuously in morphospace analyses of ammonoids (see Okamoto 1996). Ontogeny can not be fully understood in terms of the models that simply specify the gross geometry of shell coiling and aperture shape. Better understanding of the relationship between ontogenetic aspects and morphological diversity requires focusing on the geometric balance between size parameters that determines growth direction (Ubukata 2002). A promising approach for connecting the gross shell geometry with specific growth processes may lie through analysis of the profile of the band of newly accreted material around the aperture that is characterized as the "aperture map" (Rice 1998; Ubukata 2003) or a set of aperture growth vectors regulating shell coiling (Hammer and Bucher 2005b). However, a morphospace provided by the aperture map model is necessarily high-dimensional and is not practical for morphospace analysis.

This paper introduces a new theoretical model for shell growth of normally coiled ammonoids and applies it to morphospace analysis. This model is designed to simulate allometric growth of a cross-sectioned ammonoid shell. The basic assumption of the model is isometric relationship between the circumference and area of the cross-sectioned whorl; shape of the whorl section is passively regulated so as to conform the assumption. To verify the assumptions is the primary objective of this study. For this purpose, the occupation patterns of morphospace were analyzed in more than 100 Devonian to Cretaceous ammonoid species.

Institutional abbreviation.—UMUT, University Museum, University of Tokyo, Japan.

Modeling of cross-sectioned ammonoid shells

Background and basic concept.—The conventional model introduced by Raup (1967) represents growth of a planispiral shell as an expansion and rotation of a generating curve, which approximates the shape of the aperture, around a fixed coiling axis. Subsequently, Okamoto (1988) and Ackerly (1989) introduced "moving frame models" in which the amount and direction of shell growth is defined with respect to the previous aperture. Both methods conceive a shell as

the trajectory of successive generating curves that retain their shapes throughout growth. More recently, Stone (1995) proposed a "CerioShell model" defined by different expansion rates of the aperture in the horizontal and vertical dimensions for visualizing allometric change of the aperture shape and geometry of coiling. The shape of the aperture can also change if helicospiral growth is assumed for each point on the aperture (Bayer 1978; McGhee 1978; Savazzi 1987; Checa 1991; Checa and Aguado 1992) or multiple growth vectors installed around the previous aperture determine the shape of the next aperture (Hammer and Bucher 2005b).

In these previous models, no association was explicitly defined between the shape of the newly formed aperture and form of the preceding whorl. However, in normally coiled ammonoids, adjacent whorls overlap, and the soft part which formed the succeeding whorl must have covered the preceding whorl from outside. The outer component of the dorsal wall of the succeeding whorl is regarded as a product of organic secretion at the supracephalic mantle fold (Kulicki et al. 2001). Therefore, not only the shape of the previous aperture but also the form of the ventral surface of the preceding whorl should influence geometry of the newly formed aperture around the mantle margin. Hutchinson (1989) proposed a feedback mechanism in which the preceding whorl provides a "road" for the mantle margin and guides shell growth. His "road-holding model" may explain how a succeeding whorl maintains its position with respect to the preceding whorl to achieve planispiral geometry, but is not concerned with how to regulate the whorl shape. Morita (1991a, b) simulated behavior of an expanding elastic mantle represented by a finite element model of a double membrane tube. His "DMS-tube model" predicted that an expanding mantle tends to be elongated ventrally if the dorsal part of the mantle is fixed on the shell. Such mantle behavior may be a possible mechanism to regulate the whorl shape of gastropods in which the head-foot mass presses the mantle margin near the coiling axis when the snail clamps its body to the hard bottom (Morita 2003). However, this mechanism does not seem applicable to morphogenesis of nektonic ammonoids.

In the present study, we attempt to realize the process of piling up of the ammonoid whorls in which the shape of each whorl is determined in relation to the form of the preceding whorl. Therefore, the model introduced herein is based on a "moving reference frame" taking into account previous whorls and the present approach does not need the coiling axis except for measurements. The mode of accretionary growth seems to be influenced by the geometric balance of growth kinematics around the shell margin (Ubukata 2002). However, it is not easy to measure parameters from actual specimens defined by a three-dimensional model including these algorithms or developmental processes. Here, to simplify the problem, we developed a geometric model designed to simulate two-dimensional patterns which correspond to the radial cross sections of ammonoid shells. Since growth lines of ammonoid shells are not always linear or rectidi-

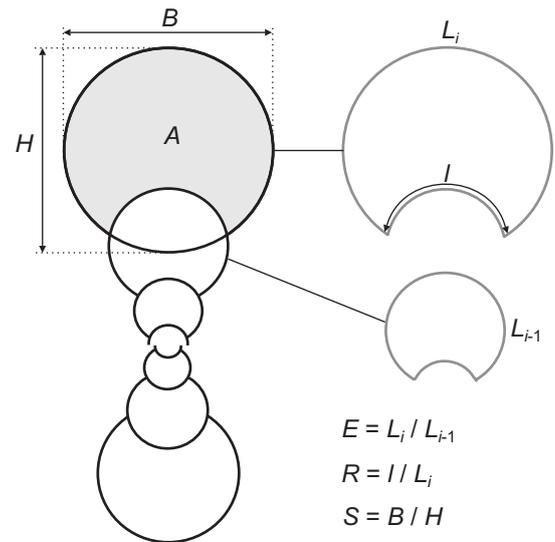

$$E = L_i / L_{i-1}$$
$$R = l / L_i$$
$$S = B / H$$

Fig. 2. Schematic figure of a cross section of the ammonoid shell showing how to define parameters of the piggyback whorls model. The enlarging rate of the whorl periphery (E) is defined as the ratio of the total perimeter of the newly added whorl section (L_i) to that of preceding whorl (L_{i-1}). The proportion of the dorsal whorl (R) is given by the ratio of the circumferential length along the dorsal wall (l) with respect to L_i. The shape of the whorl section (S) is represented by the ratio of breadth (B) and height (H) of the whorl.

radiate, a radial cross section of each whorl does not exactly represent the aperture shape but is a rough approximation of a slice of newly added shell material. Usefulness of the present geometric model can be assessed if results of computer simulations are compared with biometric data.

Piggyback whorls model.—In the cross section, growth of a normally coiled ammonoid shell is represented by additions of successive whorls: a succeessive whorl "piggybacks" on the immediately preceding one. Geometric properties of the cross-sectioned shell consist of size, shape and positional relationship between neighboring whorls. In a simple case, the cross section of the whorl is regarded as elliptic (Fig. 2). Since shelly material is secreted at the distal extremity of mantle, increase rate of the perimeter of the whorl stands for the growth rate of the mantle. If the size of each whorl is defined by the perimeter of the whorl, the growth rate in the radial direction is determined by the enlarging ratio of the perimeter with respect to the preceding whorl, E. That is,

$$L_i = EL_{i-1} \qquad\qquad (1)$$

where L_i and L_{i-1} are total perimeters of the whorl section of the succeeding and preceding whorls, respectively. Also the growth rate of body mass is reflected by the enlarging rate of the area of the cross-sectioned whorl. The ratio of the area to the perimeter influences the shape of the whorl section which is defined by the aspect ratio of the ellipse, S (see Fig. 2). In the present model, the area$^{0.5}$/perimeter ratio is assumed to be constant throughout growth as mentioned below. The positional relationship between neighboring whorls is represented by the overlap of the whorl. The whorl overlap is partly influenced by the whorl shape but is mainly determined by the proportion of
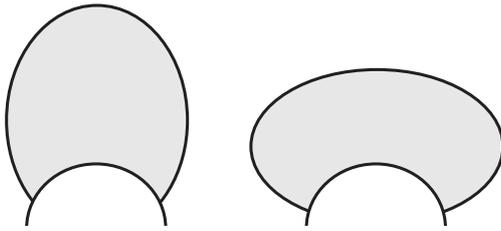
Fig. 3. Different shapes of succeeding whorl (gray area) piling up on the hemispherical preceding whorl with same L_i, l, and A values.
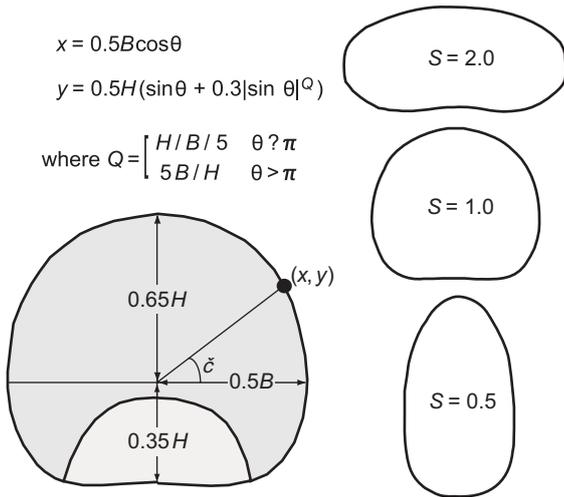

Fig. 4. Schematic diagram of an ammonoid whorl section. The shape of the whorl (S) is represented by the closed curve illustrated here which is given by the parametric equations indicated above the diagram. Figures in the right show examples of hypothetical whorl shapes with systematically varying the S value.
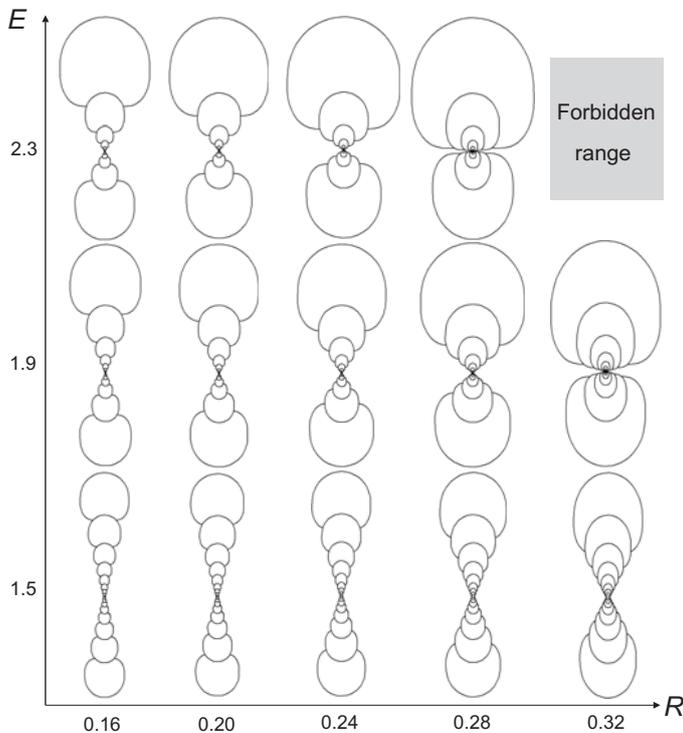

Fig. 5. Spectrum of the computer-produced ammonoids with various values of E and R when each of them is fixed throughout growth.

the circumferential length along the dorsal wall (l) to the total perimeter of the whorl section (L_i), which is expressed as R:

$$l = RL_i \qquad (2)$$

The shape of a newly added whorl, S, is dependently determined by E and R, if the preceding whorl is given and the area of the succeeding whorl in the section, A, is specified. In the default setting of the model, the initial shell consists of a pair of semicircular whorls (Fig. 2), and isometric growth of A with respect to L_i is assumed.

S depends on E and R but is not always uniquely determined by E and R. In some cases, two totally different whorl shapes are potentially generated using the same values of E and R (Fig. 3). In such cases, we chose the whorl shape which has a closer S value to the preceding whorl than the other.

In many ammonoids, the cross-sectional shape of the whorl is oval or subquadrate rather than elliptic. In computer simulations, therefore, the following parametric equations were used for producing an oval or subquadrate closed curve as a better representation of a whorl section (Fig. 4):

$$x = 0.5B\cos\theta, y = 0.5H(\sin\theta + 0.3|\sin\theta|^Q)$$

$$\text{where } Q = \begin{cases} H/B/5 & \theta \le \pi \\ 5B/H & \theta > \pi \end{cases}$$

These equations define x and y coordinates of a point on the curve at an angle θ. B and H express the breadth and height of the whorl, respectively, and S is defined as B/H. The equations above were arbitrary designed just for approximation of the whorl shape, and there is no biological basis of its formulation. Possible varieties of whorl shape can be generated with varying the value of S (Fig. 4).

We can now define shell growth in terms of shape parameters E and R, if an isometric relationship is assumed between size parameters A and L_i, and the values of E and R are fixed throughout growth. In this model, the circumferential length along the dorsal wall of the succeeding whorl ($l = RL_i$) cannot be larger than that of the external wall of the preceding whorl $[(1–R)L_i /E]$. Therefore, in the case of isometry, a theoretical model can be defined only within the following range of shape parameters:

$$E+1 \le 1/R \qquad (3)$$

In computer simulations, vast number of computer models with various shapes (S) and positions of the whorl were generated, and we searched the computer-generated models for the desired combination of L_i and A which satisfies equations (1), (2), and (3) and isometric relationship between A and L_i.

Computer simulations of shell growth

Isometric growth.—The effects of E and R on the shell form in cross section are shown on computer-produced shells in Fig. 5. When E and R are small, the model generates an
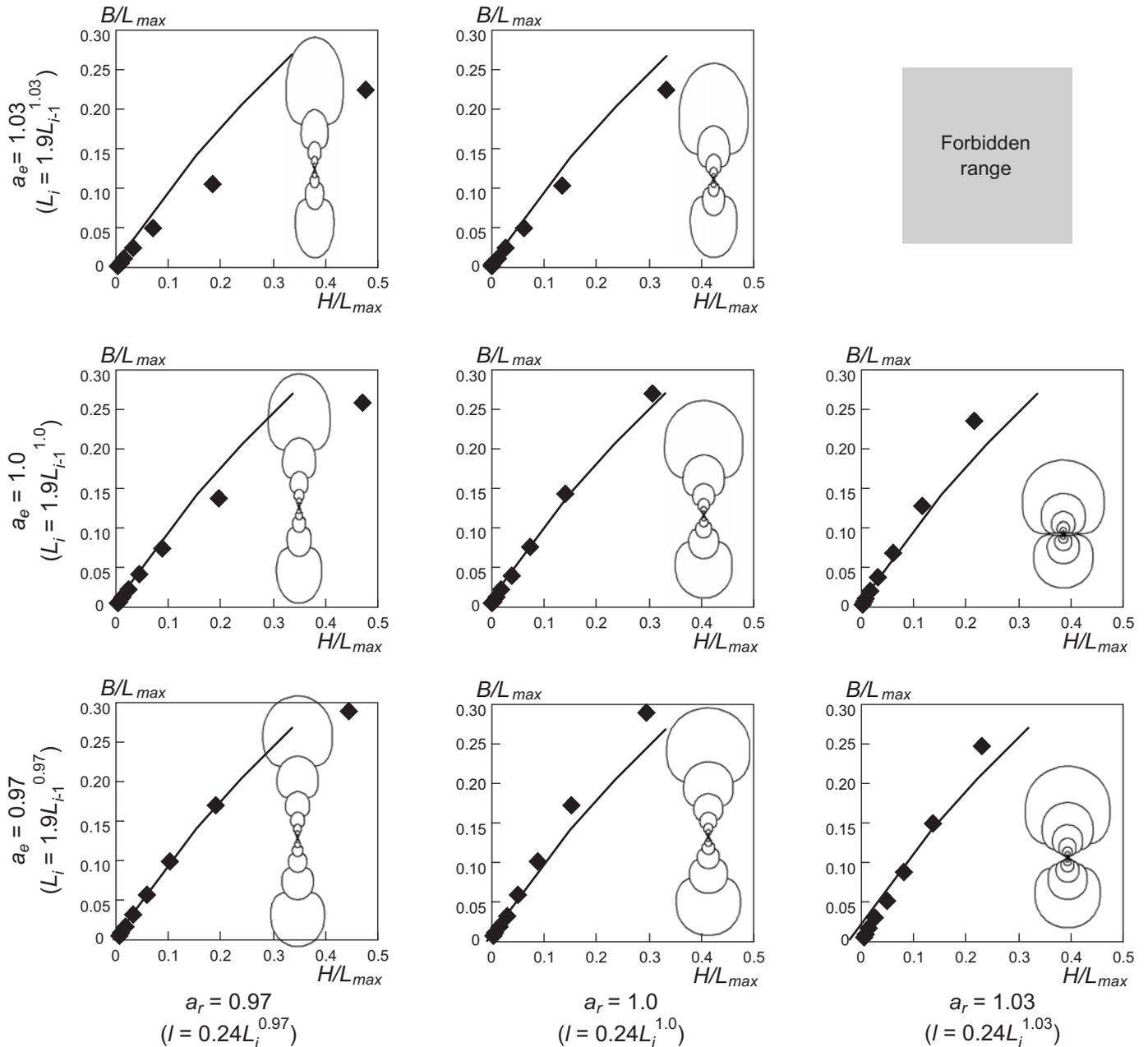
Fig. 6. Allometric growth of ammonoids. Computer models were generated with a_e and a_r values of 0.97, 1.0, and 1.3. Each diagram shows ontogenetic change in relationship between whorl height (H) and whorl breadth (B) that are standardized by the perimeter of the last whorl (L_{max}). Dashed line in each diagram represents the B/H curve in the case of isometry of E and R ($a_e = a_r = 1.0$). Note that B/H decreases with growth in the case of $a_r = 0.97$. In each model, $e = 1.9$ and $r = 0.24$.

evolute conch in which the whorls overlap little so that there is a wide umbilicus. An increase in E or R tends to produce an involute shell with a narrow umbilicus. It is a matter of course that the whorl expansion rate increases with increasing E. If E and R are too large to satisfy the former condition, any theoretical form cannot be defined in the piggyback whorls model ("forbidden range" sensu Tyszka 2006).

Theoretical models based on parameter values that are fixed throughout growth do not realize ontogenetic change in shell form. In addition, models shown in Fig. 5 do not produce variations in whorl shape: all of them have subcircular or subquadrate whorls. A greater variety can be accomplished by simulations in which E and R change with growth.

Allometric growth.—For representing allometric growth of ammonoid shells, the following equations were employed to define ontogenetic change of E and R:

$$L_i = eL_{i-1}^{ae}, \quad l = rL_i^{ar},$$

where e, r, a_e and a_r, are allometric coefficients. Parameters e and r have same effects as the enlarging ratio of the whorl perimeter and proportion of the dorsal wall respectively, and are exactly same as E and R in the case of isometry
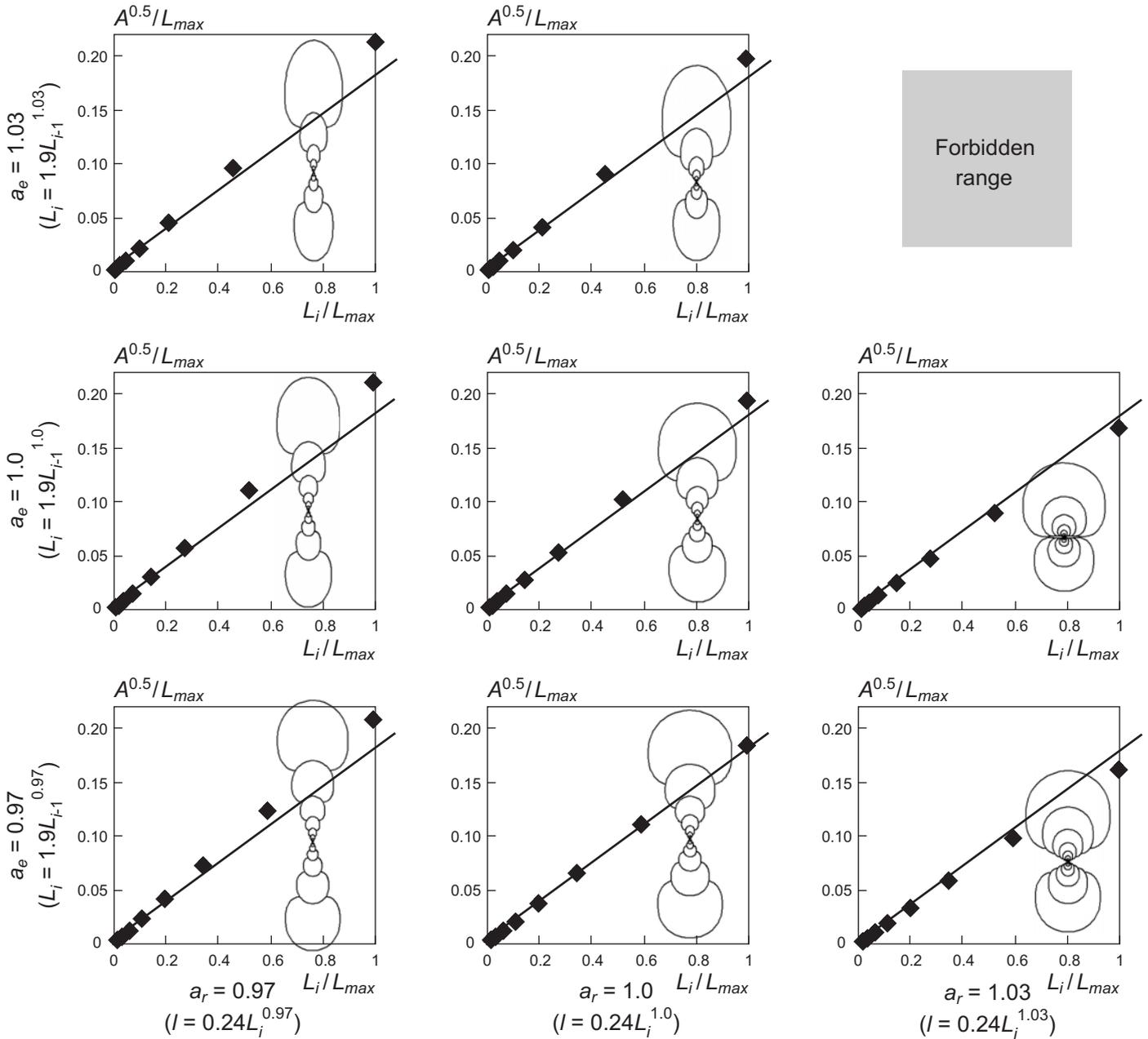
Fig. 7. Relationship between whorl perimeter (L_i) and square root of cross-sectional area of the whorl ($A^{0.5}$) which varies with a_e and a_r values. Dashed line in each diagram represents the $A^{0.5}/L_i$ curve in the case of isometry of E and R ($a_e = a_r = 1.0$). $A^{0.5}/L_i$ is generally small when a_r has a large value. In each model, $e = 1.9$ and $r = 0.24$.

(a_e=1 and a_r=1). Then, E and R are given by eL_{i-1}^{ae-1} and rL_i^{ar-1}, respectively. When $a_e>1$ or $a_r<1$, the portion of the whorl overlap decreases with growth. This condition inevitably causes an excessive area of the whorl section and results in positive allometry of A with respect to L_i, if S is fixed to 1.0 so as to maintain a subcircular or subquadrate whorl shape. In other words, isometric growth of A with respect to this condition requires reduction of S to produce a more compressed whorl, because a slender shape generally has a small $A^{0.5}/L_i$ ratio. Therefore, computer simulations in the default setting produce a slender whorl and cause a decrease of S with growth when $a_e>1$ and/or $a_r<1$ (Fig. 6).

On the contrary, when $a_e<1$ and/or $a_r>1$, the whorl overlap increases as growth proceeds, and a burly shape tends to be formed for each whorl to make up for the "deficiency" of the area (Fig. 6). However, compensation for the "deficiency" by changing the whorl shape has its limit because $A^{0.5}/L_i$ takes a maximum value around $S = 1$. If a_e is small enough or a_r is large enough, the default setting, i.e., isometric growth of A with respect to L_i, can not be held. In this case, a negative allometry was allowed in the present simulations: the maximum value of A was searched within the theoretically possible range and was employed for each whorl. Consequently, when a_e is small and a_r is large, $A^{0.5}/L_i$ tends to
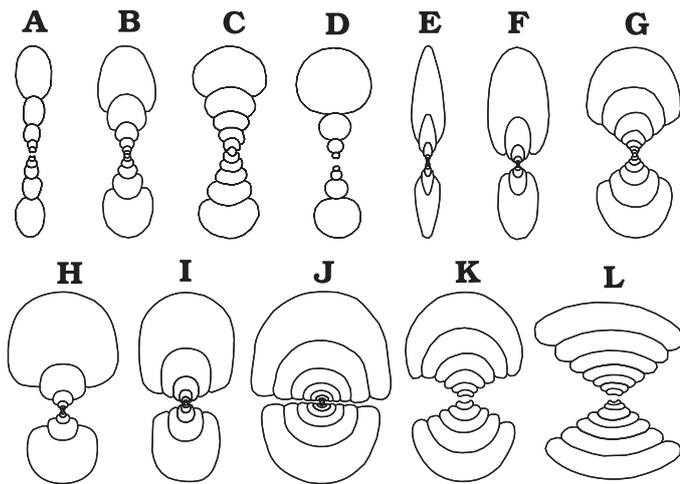
Fig. 8. Sketches of radial cross sections of ammonoids to illustrate various types of shell forms, such as planorbicone (**A**, **B**), serpenticone (**C**, **D**), oxycone (**E**), discocone (**F**), platycone (**G**, **H**), spherocone (**I**, **J**, **K**), and cadicone (**L**). **A**. *Paraceltites elegans*. **B**. *Pseudoclymenia dillensis*. **C**. *Tropigastrites lahontanus*. **D**. *Pterolytoceras* sp. **E**. *Beloceras* sp. **F**. *Phylloceras consanguineum* Gemmellaro. **G**. *Craspedites* sp. **H**. *Tetragonites glabrus*. **I**. *Damesites sugata*. **J**. *Goniatites multiliratus* Gordon. **K**. *Latanarcestes* sp. **L**. *Cabrieroceras* sp.
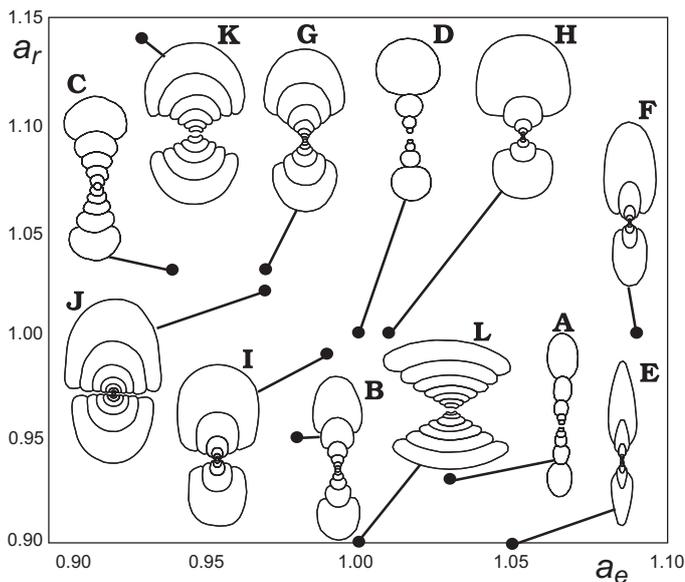

Fig. 9. Theoretical morphospace composed of a_e and a_r displaying several examples of computer-generated ammonoids that represent observed types illustrated in Fig. 8. **A**. $e = 1.5$ and $r = 0.27$. **B**. $e = 1.75$ and $r = 0.34$. **C**. $e = 2.0$ and $r = 0.17$. **D**. $e = 2.3$ and $r = 0.05$. **E**. $e = 2.0$ and $r = 0.6$. **F**. $e = 1.7$ and $r = 0.27$. **G**. $e = 1.8$ and $r = 0.24$. **H**. $e = 2.3$ and $r = 0.21$. **I**. $e = 2.3$ and $r = 0.32$. **J**. $e = 1.95$ and $r = 0.28$. **K**. $e = 1.8$ and $r = 0.10$. **L**. $e = 1.6$ and $r = 0.8$.

decrease with increasing size so that it has a smaller value in comparison with other cases (Fig. 7). If *ae* and *ar* are both considerably larger than zero, any theoretical form cannot be defined.

If appropriate values of a_e and a_r are used with various combinations of *e* and *r*, many varieties of shell forms observed in actual ammonoids as shown in Fig. 8, can be pro-

duced (Fig. 9). An evolute conch with a compressed whorl, or planorbicone, is generated when a_r is small and a_e is around 1.0 (Fig. 9A, B). A model with a large value of a_e can produce a discoidal form with a compressed whorl and a narrow umbilicus (Fig. 9F). A spheroconic shell which is characterized by a subglobular whorl and involute coiling is readily reproduced when a_r is around one and a_e is slightly smaller than 1.0 (Fig. 9G, I, J). If *r* is large and a_r is small, a theoretical model possessing a large value of *e* tends to generate an oxyconic form with an extremely compressed whorl (Fig. 9E), while a model with a small *e* value can produce a cadiconic form with a depressed whorl (Fig. 9L). Other observed forms, such as are seen in Fig. 1C, D, H, K, can be generated by our model (Fig. 9C, D, H, K).

Morphospace analysis

Computer simulations.—The piggyback whorls model assumes that the shape of a whorl section depends on the balance between the perimeter and area of the whorl section. This assumption may cause biased occupation patterns of theoretically possible forms in the morphospace which defines the relationship between growth parameters and cross-sectional form. If so, analysis of the distribution of actual forms in relation to the theoretical morphospace allows us to test the assumption. Since allometric growth is defined by *e*, *r*, a_e and a_r, the morphospace composed of these growth parameters and a dependent subsidiary parameter such as *S* should be high-dimensional. Since accurate estimations of *e* and *r* from specimens are not easy, the relationship between pairs of a_e and a_r and subsidiary parameters including Raup's ones was analyzed to assess explicability of the piggyback whorls model for well-known correlations among Raup's parameters.

In addition to *S*, the following three subsidiary parameters were also assessed: whorl expansion rate, W_c; width of umbilicus, or Raup's *D* (Fig. 10); and ratio of the square root of the area to the perimeter, $A^{0.5}/L_i$. Raup (1967) defined the whorl expansion rate as the rate of increase in the diameter of an ammonoid shell per revolution: it can be defined independent of *S* in the case of isometry. However, increase in compression of the whorl during growth results in increase in the whorl expansion rate defined by Raup (1967). In this study, for avoidance of algebraic dependency, W_c was defined as the ratio of the distance from the coiling axis to the center of a given whorl to that of the preceding one (Fig. 10). The center of the whorl is defined as the point on the median line equally distant from the ventral and dorsal extremes of the whorl. When $a_e <> 1$ or $a_r <> 1$, the values of *S*, W_c, *D*, and $A^{0.5}/L_i$ generally change with growth. In the present analysis, these subsidiary parameters were estimated for the latest whorl both in theoretical models and actual specimens.

Computer simulations were performed to establish theoretical morphospaces composed of a_e, a_r, and *S*, W_c, *D* or

$$D = \frac{d_1}{d_2}$$

$$W_c = \frac{c_2}{c_1}$$
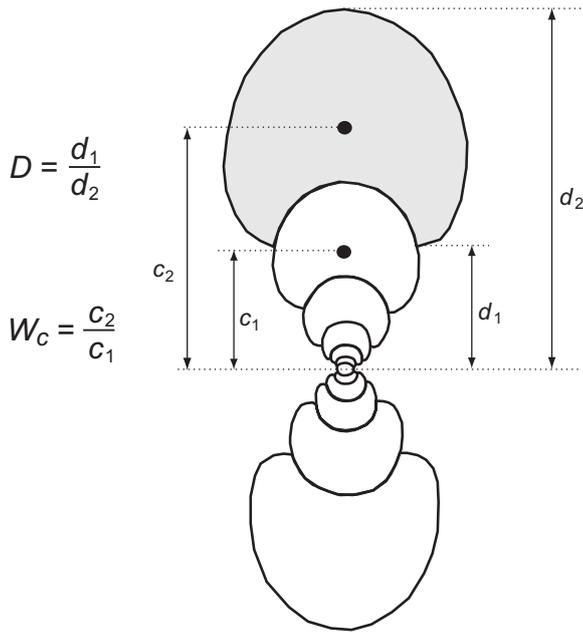
Fig. 10. Measurements of the whorl expansion rate (W_c) and width of umbilicus (D). Note that c_1 and c_2 are defined as the distances from the coiling axis to the centers of the whorls. d_1 and d_2 are distances of umbilical seams from the coiling axis.

$A^{0.5}/L_i$ with various values of e, r, a_e, and a_r. A total of 200 theoretical models were simulated. In each model, values of e, r, a_e and a_r were randomly chosen from the normally distributed populations with the following means and standard deviations: $\mu = 2$, $\sigma = 0.2$ for e; $\mu = 0.25$, $\sigma = 0.05$ for r; $\mu = 1$, $\sigma = 0.05$ for a_e and a_r. The subsidiary parameters associated with each combination of a_e and a_r attain various values depending on e and r, but are obviously correlated with a_e and/or a_r (Fig. 11A–D). S tends to decrease as a_r decreases or a_e increases (Fig. 11A). In this case, a_r is the predominant factor in determination of the shape parameters. On the other hand, $A^{0.5}/L_i$ generally increases with decreasing a_r (Fig. 11B). As mentioned above, a small a_r or large a_e value reduces the portion of the whorl overlap with growth and potentially yields an excessive area of the whorl section to increase $A^{0.5}/L_i$ (Fig. 11B). In this condition, balancing between A and L_i reduces the value of S to produce a compressed whorl (Fig. 11A). W_c dominantly depends on a_e (Fig. 11C), and this relation is rather obvious: a large a_e value readily causes a large whorl expansion rate. D has a tendency to decrease with increase either of a_e or a_r, but is mainly influenced by a_r (Fig. 11D). As a natural consequence of comparison of morphospaces between Fig. 11A and Fig. 11C, a clear negative correlation between S and W_c was generated in our computer simulations (Fig. 11E). For a similar reason, there is a positive correlation between S and D (Fig. 11F), and consequently a negative one between S and W_c, which have been reported in many ammonoids (Bayer and McGhee 1984; Saunders and Swan 1984; Swan and Saunders 1987; Dommergues et al. 1996; Saunders and Work 1996). These

correlations derived from the assumption of the piggyback whorls model: balancing between A and L_i determines S.

Biometric analyses.—The occupation patterns of hypothetical models in the morphospaces shown in Fig. 11 were compared with the distribution of actual ammonoids to test our assumption. To assess the pattern of morphological diversity of actual ammonoids, a_e, a_r, S, W_c, D and $A^{0.5}/L_i$ were estimated on 123 specimens of 115 species, belonging to 72 families (see Appendix 1). Since each species was represented by one or a few specimen, the present analyses and following discussions basically dealt with shape variation above species level. Our material covers six ammonoid orders spanning from the Devonian to the Cretaceous.

Each specimen was first cut using an electric diamond saw vertical to the median plane. The half section was polished with graded series of silicon-carbide powders along the radial plane. A sheet of cellophane tape was pressed onto the polished surface to make the structure on the surface clearly visible. The polished surface was laid onto the image scanner (Epson GT-F600), and an image of the surface was captured and saved as a computer bitmap file. Two-dimensional coordinate data along the periphery of the whorl were collected on the bitmap image using a digitizing program written in Visual Basic 6.0 (Ubukata 2004, 2005), and then, the perimeter along the sectioned whorl was calculated. We measured to the outside of the shell wall because morphogenesis of the external shell surface is not affected by shell thickening. The height, breadth and center of the whorl were determined by the coordinate data to obtain S, D and W. For measuring A, the periphery of each whorl was traced and colored differently on a personal computer using Justsystem Hanako PhotoRetouch 2004 program, and its area was measured by counting pixels (Ubukata 2001). For this counting, a program written in Visual Basic 6.0 was used. Consequently, a_e and a_r were obtained as slopes of reduced major axes of $\log L_i$ against $\log L_{i-1}$, and $\log l$ against $\log L_i$, respectively (Jones 1937). For details of the regression method using the reduced major axis, refer also to Imbrie (1956). Multiple regression analyses were conducted for parameters on a_e and a_r.

The range of forms of actual ammonoids examined was consistent with the occupation patterns of theoretical models in morphospace shown in Fig. 11. In actual ammonoids, S appears to decrease with increase of a_e or decrease of a_r in Fig. 12A. A multiple regression analysis revealed a significant negative partial correlation between a_e and S, and a positive correlation between ar and S, and the latter is especially prominent (Table 1). Fig. 11B indicates a negative relationship between $A^{0.5}/L_i$ and a_r, and a multiple regression analysis provided a significant trend to decreasing $A^{0.5}/L_i$ as a function of a_r (Table 1). The value of W_c seems to increase as a_e increases (Fig. 12C), which was supported by multiple regression analysis (Table 1). A significant negative partial correlation was found between a_r and D (Table 1, Fig. 12D). Biometric analyses also revealed a clear negative or inverse relationship between S and W_c (Fig. 12E) and a week positive correlation be-
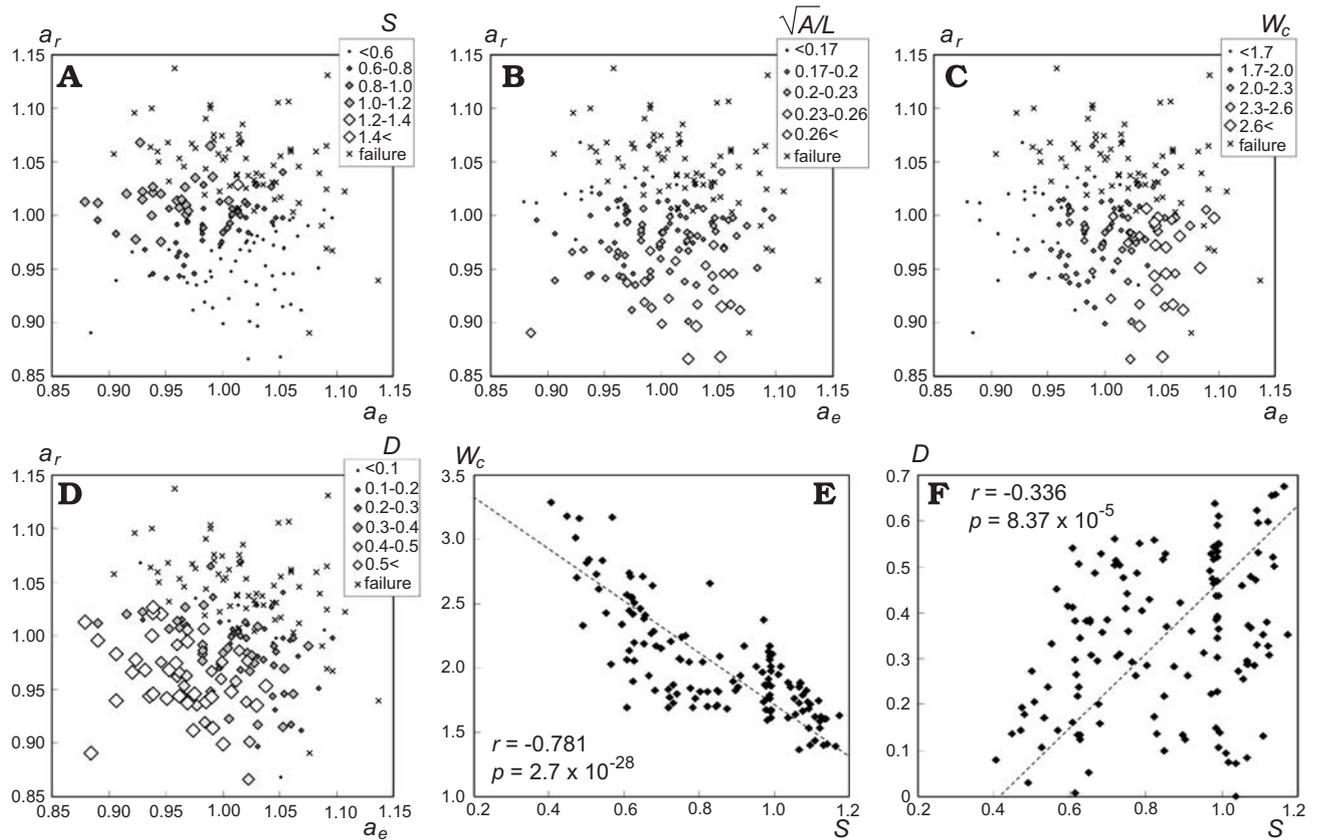
Fig. 11. Results of computer simulations. A–D, theoretical morphospaces based on the piggyback whorls model composed of a_e and a_r showing values of shape parameters (S, $A^{0.5}/L_i$, W_c, D) of a theoretical model corresponding to each combination of a_e and a_r. E, negative correlation between W_c and S values obtained from theoretical models. F, positive correlation between D and S. The values of S, $A^{0.5}/L_i$, W_c or D are exhibited by the size of the plots, and × indicates that a "forbidden" combinations of a_e, a_r, e, and r was employed in each simulation resulting in failure of defining form (A–D).

Table 1. Results of multiple regression analyses.

Regression of		Standard partial regression coefficient	Partial correlation coefficient	p
S	ae	-0.3319	-0.3362	0.0002
	ar	0.2220	0.2323	0.0100
W	ae	0.2860	0.2887	0.0013
	ar	-0.2237	-0.2295	0.0110
$A^{0.5}/L$	ae	0.0509	0.0650	0.4769
	ar	-0.6430	-0.6352	0.0000
D	ae	-0.0849	-0.0891	0.3294
	ar	-0.4209	-0.4053	0.0000

tween S and D (Fig. 12F). These results are generally concordant with results of computer simulations (Fig. 11), and thus support the assumption of the present model.

Discussion

Correlations among Raup's parameters.—Saunders and Swan (1984) and Swan and Saunders (1987) analyzed Raup's W-D-S morphospace in various Paleozoic ammonoids and identified correlations among these parameters that are not ex-

plicable in terms of hydrodynamics or hydrostatics: a negative correlation between W and D, and a positive one between S and D, that have been confirmed by several authors (Bayer and McGhee 1984; Dommergues et al. 1996; Saunders and Work 1996), and were also reconfirmed in the present study. Swan and Saunders (1987) suggested that these correlations originated in restrictions imposed by the relative aperture height and aperture area with respect to shell size. They found that the major axis of plots was distributed along aperture-height curves in the W-D morphospace and S-D plots run parallel to aperture-area curves (Swan and Saunders 1987: figs. 8, 9). Swan and Saunders (1987) supposed preferences for aperture height and aperture area that make a moderately deep U-shaped cross section to avoid biomechanical disadvantages.

In the present piggyback whorls model, isometric relationship is assumed between the area of the whorl cross section and the whorl perimeter. It may be safe to say that this assumption of the model is concordant with the Swan and Saunders (1987) hypothesis of restrictions on aperture height and aperture area. The piggyback whorls model displayed how constructional bias imposed by the area of whorl section work on the occupation pattern of morphospace: changing the geometry of shell coiling inevitably results in change in the aperture shape so as to keep the constant relative area of
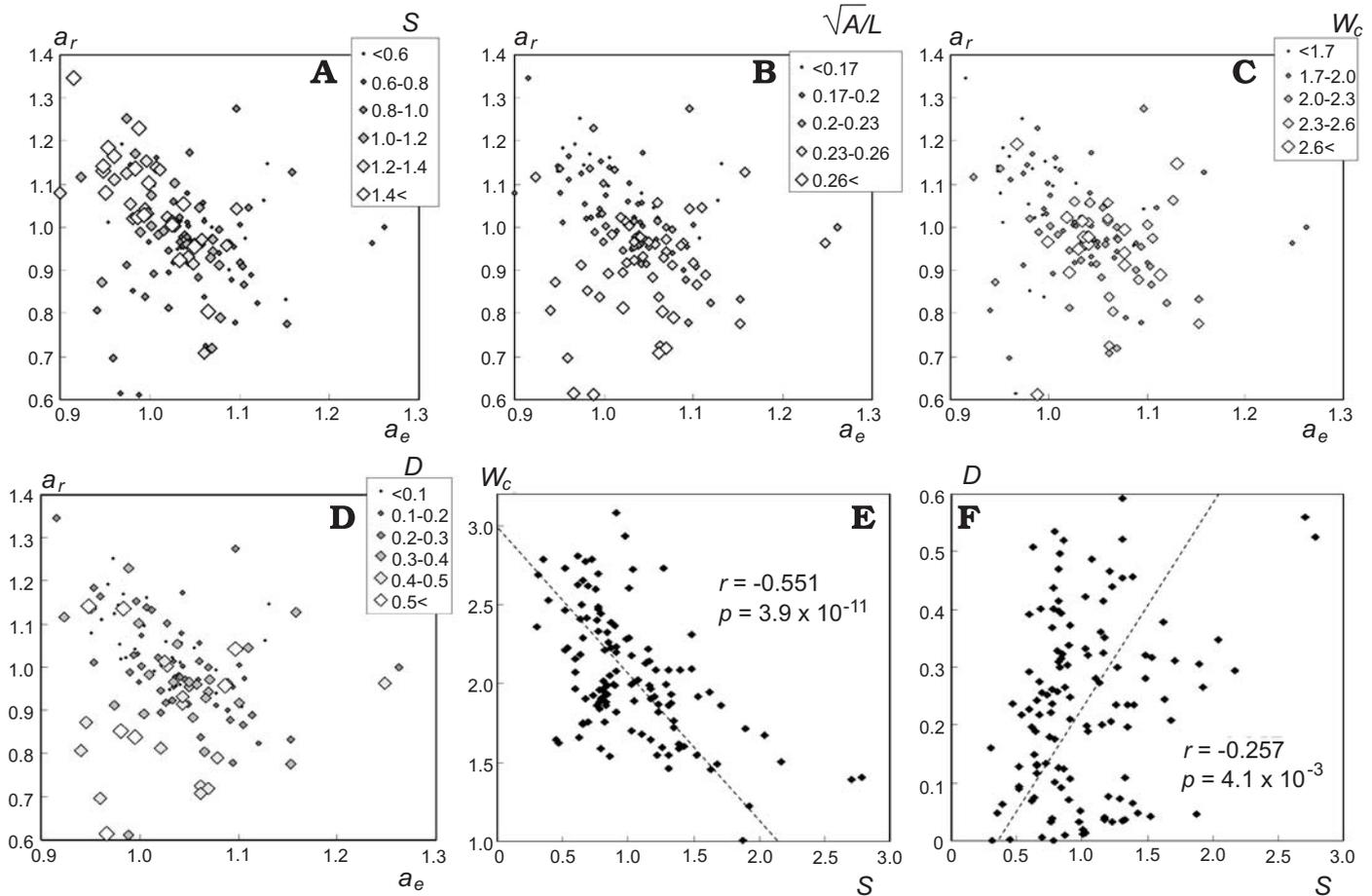
Fig. 12. The same morphospaces as Fig. 11 showing the distribution of 115 species based on measurements.

the aperture with respect to its perimeter. Since the values of Raup's parameters depend on r and a_r, correlations among Raup's parameters can be regarded as axiomatic consequences of algebraic interdependence among them, if an isometric relationship is assumed between the area and perimeter of the whorl cross section. Concerning the Raup's model, Schindel (1990) pointed out that, the dorsal shell margin of two whorls can move away from the coiling axis at the same rate but with different D values, because of an algebraic interdependence between W and D under a fixed displacement rate of the dorsal shell margin (see also Stone 1996). Origination of a correlation between parameters from an assumed condition (e.g., fixed displacement rate, or isometry between area and perimeter) can be attributed to a simple mathematical problem; however, the assumed condition should be placed in a biological context. In the case of the present study, correlations among Raup's parameters may be interpreted as "constructional linkages" associated with particular configurations of aperture height and aperture area that were assumed by Swan and Saunders (1987).

Buckman's Law of Covariation.—The piggyback whorls model may partly explain Buckman's Law of Covariation between ornament and shell shape: strongly ornamented am-

monoids tend to have an evolute conch and circular whorls (Westermann 1966). This "law" has been confirmed by the morphologic analysis of large population samples of some Triassic ceratites (Dagys and Weitschat 1993; Dagys et al. 1999; Dagys, 2001) and a Cretaceous ammonite *Neogastroplites* (Kennedy and Cobban, 1976), and this phenomenon has been explained in terms of a reaction diffusion model (Guex et al. 2003) and a simple principle of proportionality (Hammer and Bucher 2005a).

If an ornamented closed curve is *a priori* given for whorl cross section as an initial setting, same computer simulations as shown in Fig. 11D tend to generate more depressed whorls with larger S values in the piggyback whorls model (Fig. 13), where compression is *a posteriori* determined. In terms of the piggyback whorls model, formation of heavy ornaments makes a long periphery of the whorl and reduces the $A^{0.5}/L_i$ ratio. In this case, employing a circular aperture maximizes the area of the whorl section and then balances between A and L_i, as in the case that a burly aperture makes up for the deficiency of the area caused by increase of the whorl overlap with growth (Fig. 6). Since shell involution is practically determined by r and a_r that are *a priori* given in the present simulations, the relationship between evolute conch and ornamentation was not reproduced.
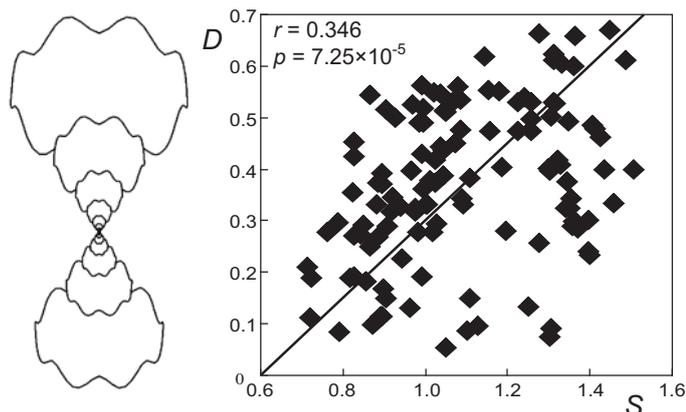
Fig. 13. Results of same computer simulations as shown in Fig. 11 with an ornamented whorl shape. In order to produce an ornamented closed curve, the following parametric equations were used: $x = 0.5B\cos\theta$, $y = 0.5H(\sin\theta + 0.3|\sin4\theta|Q)$, where $Q = H/B/5$ if $\theta \leq \pi$, while $Q = 5B/H$ if $\theta > \pi$. Note that simulated S values tend to be large as compared with Fig. 11F.

Yacobucci (2004) found that Cretaceous acanthoceratid ammonites with highly variable shell shapes did not show variable patterns of ornamentation, although the Buckman's Law should expect a positive correlation of variations between shell shape and rib features. She suggested that ornament morphogenesis is genetically and/or developmentally more controlled than is shell shape. If gross shell geometry is more variable than shell sculpture, heavy ornamentation which may lead changes in whorl shape. However, this explanation based on the present model can only be applied to tubercles and spiral ribs, because radial ribbing involves little change in aperture shape, which in turn does not influence $A^{0.5}/L_i$.

Hydrostatics and hydrodynamics.—As a result of computer simulations based on the piggyback whorls model, we expected that positive allometry of whorl periphery causes the whorl to become more slender and more rapidly expanding (Fig. 11A, C). Morphometric analysis also found that the allometric coefficient of periphery is negatively correlated with whorl compression but is positively correlated with whorl expansion rate (Fig. 12A, C, Table 1). Positive allometry of the whorl periphery means acceleration of the lateral expansion of the soft body. If this is not attended with acceleration of increase in total soft-body mass, body-chamber length is necessarily shortened to compensate rapid expansion of the diameter. Therefore, the process of building a compressed whorl with a high expansion rate may result in formation of a short body chamber. This study did not examine the body-chamber length because most of the specimens utilized did not preserve the entire body chamber. However, a negative correlation between body-chamber length and whorl expansion rate has been observed in some taxa (Okamoto 1996; Klug and Korn 2004). From the view point of hydrostatics, this correlation is theoretically expected if neutral buoyancy is presumed (Saunders and Shapiro 1986; Ebel 1990). The piggyback whorls model may explain how ammonoids constructed neutrally buoyant shell morphology;

constraints imposed by the relative area of the aperture with respect to its perimeter may cause a negative correlation between body-chamber length and whorl expansion rate.

In addition, a negative correlation between S and whorl expansion rate (Fig. 12E) strongly suggests a negative correlation between whorl compression and body chamber length. A shell with a short body chamber has high hydrostatic stability which allows the animal's fast locomotion without rotation (Trueman 1941; Raup 1967; Saunders and Shapiro 1986; Ebel 1990; Okamoto 1996). In terms of hydrodynamics, a compressed form generally has a lower drag coefficient than robust one. However, a compressed shell has a smaller amount of retractor muscle and a larger surface area which generates a larger frictional drag than a thicker form. Thus, the compressed form is effective for reducing drag only at a high Reynolds number which represents a large size and/or a fast swimming velocity (Jacobs 1992; Jacobs and Chamberlain 1996; Seki et al. 2000). Positive allometry of whorl periphery readily realizes an ideal coupling of morphological characters for a fast-swimming ammonite, because of the constructional linkage between whorl compression and whorl expansion rate. Furthermore, it also results in an ontogenetic change from a less compressed to more compressed shape: such ontogenetic trend is suitable for swimming because smaller forms that swim slowly benefit from less compressed shapes (Jacobs 1992; Jacobs and Chamberlain 1996).

In general terms, this study suggests that constructional biases as assumed in the piggyback whorls model can provide a functional coupling of morphological characters. Functional and developmental integrations of characters have been focused in the context of developmental constraints (Alberch 1980, 1982; Kauffman 1983; Schwenk and Wagner 2001; Richardson and Chipman 2003), and have been discussed from viewpoints of pleiotropy (Cheverud 1996; Raff 1996; Adams 1998; Moore et al. 2004; Klingenberg 2005) or epigenetic processes (Müller 1989; Morita 1993). Although this study did not attempt to elucidate developmental mechanism of morphogenesis of functionally coupling characters, the piggyback whorls model expects "constructional linkages" between aperture shape and coiling geometry.

Concluding remarks and prospects

The piggyback whorls model introduced for mimicking ammonoid shell growth is based on the geometric balance among perimeters of the external and internal portions and area of the whorl section. The balance determines degree of compression and involution of whorls. None of the growth parameters used in this model directly defines the shape of the aperture and geometry of shell coiling. Theoretical forms generated by using the piggyback whorls model has a potential to explain well-known correlations among whorl expansion rate, width of umbilicus and whorl shape (Fig. 11E, F), as consequences from constructional biases imposed by isometric relationship between perimeter and area of the whorl cross section.

The piggyback whorls model is not designed to simulate openly coiled or uncoiled form, because it attributes great variation in aspect ratio of whorl section to ontogenetic change of whorl overlap and whorl expansion rate. The present model is not comprehensive enough to reproduce various teratological patterns observed in actual ammonoids. In addition, it is not sufficient for analysis of the three-dimensional properties of shell form. The model does not address the effect of pattern of relative growth rate around the aperture on the aperture shape. Combining the present model with the aperture map model (Rice 1998) or aperture growth vector model (Hammer and Bucher 2005b) may be required to show how three-dimensional shell form is determined.

Nevertheless, the present model is useful for analysis of ontogenetic variation of ammonoids, which is usually based on cross sections of shells. There is a prospect that the model may explain how to realize a functional coupling between hydrostatic and hydrodynamic characters and how to produce the Buckman's Law of Covariation between rib features and shell shapes. The approach introduced here is also available for studies on nautilids, and might be applicable to gastropod shell morphology after some necessary modifications.

Acknowledgments

References

Ackerly, S.C. 1989. Kinematics of accretionary shell growth, with examples from brachiopods and molluscs. *Paleobiology* 4: 374–378.

Adams, R.A. 1998. Evolutionary implications of developmental and functional integration in bat wings. *Journal of Zoology* 246: 165–174.

Alberch, P. 1980. Ontogenesis and morphological diversification. *American Zoologists* 20: 653–667.

Alberch, P. 1982. Developmental constraints in evolutionary processes. *In*: J.T. Bonner (ed.), *Evolution and Development*, 313–332. Springer-Verlag, Berlin.

Bayer, U. 1978. Morphologenetic programs, instabilities, and evolution—a theoretical study. *Neues Jahrbuch für Geologie und Paläontologie, Abhandlungen* 156: 226–261.

Bayer, U. and McGhee, J.R. Jr. 1984. Iterative evolution of Middle Jurassic ammonite faunas. *Lethaia* 17: 1–16.

Bogoslovskaya, M.F. [Bogoslovskaâ, M.F.], Kuzina, L.F., and Leonova, T.B. 1999. Classification and distribution of late Paleozoic ammonoids [in Russian, with English abstract]. *In*: A.Û. Rozanov and A.A. Ševyrev (eds.), *Iskopaemye cefalopody: novejšie dostiženiâ v ih izučenii*, 89–124. Paleontologičeskij Institut, Rossijskajâ academiâ nauk, Moskva.

Checa, A. 1991. Sectorial expansion and shell morphogenesis in molluscs. *Lethaia* 24: 97–114.

Checa, A. and Aguado, R. 1992. Sectorial-expansion analysis of irregularly coiled shells; application to the Recent gastropod *Distorsio*. *Palaeontology* 35: 913–925.

Cheverud, J.M. 1996. Developmental integration and the evolution of pleiotropy. *American Zoologists* 36: 44–50.

Dagys, A.S. 2001. The ammonoid family Arctohungaritidae from the Boreal Lower-Middle Anisian (Triassic) of Arctic Asia. *Revue Paléobiologie, Genève* 20: 543–641.

Dagys, A.S., Bucher, H., and Weitschat, W. 1999. Intraspecific variation of *Parasibirites kolymensis* Bychkov (Ammonoidea) from the Lower Triassic (Spathian) of Arctic Asia. *Mitteilungen Geologisches-Paläontologisches Institut Universität Hamburg* 83: 163–178.

Dagys, A.S. and Weitschat, W. 1993. Extensive intraspecific variation in a Triassic ammonoid from Siberia. *Lethaia* 26: 113–121.

Dommergues, J-L., Laurin, B., and Meister, C. 1996. Evolution of ammonoid morphospace during the Early Jurrasic radiation. *Paleobiology* 22: 219–240.

Ebel, K. 1990. Swimming abilities in ammonites and limitations. *Paläontologische Zeitschrift* 64: 25–37.

Gottobrio, W.E. and Saunders, W.B. 2005. The clymeniid dilemma: functional implications of the dorsal siphuncle in clymeniid ammonoids. *Paleobiology* 31: 233–252.

Guex, J., Koch, A., O'Dogherty, L., and Bucher, H. 2003. A morphogenetic explanation of Buckman's law of covariation. *Bulletin de la Société géologiaue de France* 174: 603–606.

Hammer, Ø. and Bucher, H. 2005a. Buckman's first law of covariation—a case of proportionality. *Lethaia* 38: 67–72.

Hammer, Ø. and Bucher, H. 2005b. Models for the morphogenesis of the molluscan shell. *Lethaia* 38: 111–122.

Hutchinson, J.M.C. 1989. Control of gastropod shell shape: the role of the preceding whorl. *Journal of Theoretical Biology* 140: 431–444.

Imbrie, J. 1956. Biometrical methods in the study of invertebrate fossils. *Bulletin of the American Museum of Natural History* 108: 217–252.

Jacobs, D.K. 1992. Shape, drag, and power in ammonoid swimming. *Paleobiology* 18: 203–220.

Jacobs, D.K. and Chamberlain, J.A. Jr. 1996. Buoyancy and hydrodynamics in ammonoids. *In*: N.H. Landman, K. Tanabe, and R.A. Davis (eds.), *Ammonoid Paleobiology*, 169–224. Plenum, New York.

Jones, H.E. 1937. Some geometrical considerations in the general theory of fitting lines and planes. *Metron* 13: 21.

Kauffman, S.A. 1983. Developmental constraints: internal factors in evolution. *In*: B. Goodwin, N. Holder, and C.C. Wiley (eds.), *Development and Evolution*, 195–225. Cambridge University Press, Cambridge.

Kennedy, W.J. and Cobban, W.A. 1976. Aspects of ammonite biology, biogeography, and biostratigraphy. *Special Papers in Palaeontology* 17: 1–94.

Klingenberg, C.P. 2005. Developmental constraints, nodules, and evolvability. *In*: B. Hallgrímsson and B.K. Hall (eds.), *Variation: A Central Concept in Biology*, 219–249. Academic Press, San Diego.

Klug, C. and Korn, D. 2004. The origin of ammonoid locomotion. *Acta Palaeontologica Polonica* 49: 235–242.

Korn, D. 2000. Morphospace occupation of ammonoids over the Devonian–Carboniferous boundary. *Paläontologische Zeitschrift* 74: 247–257.

Korn, D. and Klug, C. 2002. *Ammoneae Devonicae*. *In*: W. Riegraf (ed.), *Fossilum Catalogus I: Animalia Pars 138*. 375 pp. Backhuys, Leiden.

Korn, D. and Klug, C. 2003. Morphological pathways in the evolution of Early and Middle Devonian ammonoids. *Paleobiology* 29: 329–348.

Kulicki, C., Tanabe, K., Landman, N.H., and Mapes, R.H. 2001. Dorsal shell wall in ammonoids. *Acta Palaeontologica Polonica* 46: 23–42.

McGhee, G.R. Jr. 1978. Analysis of the shell torsion phenomenon on the Bivalvia. *Lethaia* 11: 315–329.

McGowan, A.J. 2004. The effect of the Permo-Triassic bottleneck on Triassic ammonoid morphological evolution. *Paleobiology* 30: 369–395.

Morita, R. 1991a. Finite element analysis of a double membrane tube (DMS-tube) and its implication for gastropod shell morphology. *Journal of Morphology* 207: 81–92.

Morita, R. 1991b. Mechanical constraints on aperture form in gastropods. *Journal of Morphology* 207: 93–102.

Morita, R. 1993. Development mechanics of retractor muscles and the "Dead Spiral Model" in gastropod shell morphogenesis. *Neues Jahrbuch für Geologie und Paläontologie, Abhandlungen* 190: 191–217.

Morita, R. 2003. Why do univalve shells of gastropods coil so tightly? A head-foot guidance model of shell growth and its implication on developmental constraints. *In*: T. Sekimura, S. Noji, N. Ueno, and P.K. Maini (eds.), *Morphogenesis and Pattern Formation in Biological Systems: Experiments and Models*, 345–354. Springer-Verlag, Tokyo.

Moore, P.J., Harris, W.E., Montrose, V.T., Levin, D., and Moore, A.J. 2004. Constraints on evolution and postcopulatory sexual selection: trade-offs among ejaculate characteristics. *Evolution* 58: 1773–1780.

Müller, G.B. 1989. Ancestral patterns in bird limb development: a new look at Hampé's experiment. *Journal of Evolutionary Biology* 2: 31–47.

Nikolaeva, S.V. and Barskov, I.S. 1994. Morphogenetic trends in the evolution of Carboniferous ammonoids. *Neues Jahrbuch für Geologie und Paläontologie, Abhandlungen* 193: 401–418.

Okamoto, T. 1988. Analysis of heteromorph ammonoids by differential geometry. *Palaeontology* 31: 35–52.

Okamoto, T. 1996. Theoretical modeling of ammonoid morphology. *In*: N.H. Landman, K. Tanabe, and R.A. Davis (eds.), *Ammonoid Paleobiology*, 225–251. Plenum, New York.

Page, K.N. 1996. Mesozoic ammonoids in space and time. *In*: N.H. Landman, K. Tanabe, and R.A. Davis (eds.), *Ammonoid Paleobiology*, 755–794. Plenum, New York.

Raff, R.A. 1996. *The Shape of Life: Genes, Development, and the Evolution of Animal Form*. 544 pp. University of Chicago Press, Chicago.

Raup, D.M. 1967. Geometric analysis of shell coiling: coiling in ammonoids. *Journal of Paleontology* 41: 43–65.

Rice, S.H. 1998. The bio-geometry of mollusk shells. *Paleobiology* 24: 133–149.

Richardson, M.K. and Chipman, A.D. 2003. Developmental constraints in a comparative framework: a test case using variations in phalanx number during amniote evolution. *Journal of Experimental Zoology Part B: Molecular and Developmental Evolution* 296: 8–22.

Saunders, W.B. and Shapiro, E.A. 1986. Calculation and simulation of ammonoid hydrodynamics. *Paleobiology* 12: 64–79.

Saunders, W.B. and Swan, A.R.H. 1984. Morphology and morphological diversity of mid-Carboniferous (Namurian) ammonoids in time and space. *Paleobiology* 10: 195–228.

Saunders, W.B. and Work, D.M. 1996. Shell morphology and suture complexity in Upper Carboniferous ammonoids. *Paleobiology* 22: 189–218.

Saunders, W.B. and Work, D.M. 1997. Evolution of shell morphology and suture complexity in Paleozoic prolecanitids, the rootstock of Mesozoic ammonoids. *Paleobiology* 23: 301–325.

Saunders, W.B., Work, D.M., and Nikolaeva, S.V. 2004. The evolutionary history of shell geometry in Paleozoic ammonoids. *Paleobiology* 30: 19–43.

Savazzi, E. 1987. Geometric and functional constraints on bivalve shell morphology. *Lethaia* 20: 293–306.

Schindel, D.E. 1990. Unoccupied morphospace and the coiled geometry of gastropods: architectural constraint or geometric covariation? *In*: R.M. Ross and W.D. Allmon (eds.), *Causes of Evolution: A Paleontological Perspective*, 270–304. University of Chicago Press, Chicago.

Schwenk, K. and Wagner, G.P. 2001. Function and evolution of phenotypic stability: connecting pattern to processes. *American Zoologists* 41: 552–563.

Seki, K., Tanabe, K., Landman, N.H., and Jacobs, D.K. 2000. Hydrodynamic analysis of Late Cretaceous desmoceratine ammonites. *Revue Paléobiologie, Genève, Volume spéciale* 8: 141–155.

Stone, J.R. 1995. CerioShell: a computer program designed to simulate variation in shell form. *Paleobiology* 21: 509–519.

Stone, J.R. 1996. The evolution of ideas: a phylogeny of shell models. *The American Naturalist*, 148: 904–929.

Swan, A.R.H. and Saunders, W.B. 1987. Function and shape in late Paleozoic (mid-Carboniferous) ammonoids. *Paleobiology* 13: 297–311.

Trueman, A.E. 1941. The ammonite body-chamber, with special reference to the buoyancy and mode of life of the living ammonite. *Quaternary Journal of the Geological Society of London* 96: 339–383.

Tyszka, J. 2006. Morphospace of foraminiferal shells: results from the moving reference model. *Lethaia* 39: 1–12.

Ubukata, T. 2001. Geometric pattern and growth rate of prismatic shell structures in Bivalvia. *Paleontological Research* 5: 33–44.

Ubukata, T. 2002. Stacking increments: a new model and morphospace for the analysis of bivalve shell growth. *Historical Biology* 15: 303–321.

Ubukata, T. 2003. Pattern of growth rate around aperture and shell form in Bivalvia: a theoretical morphological study. *Paleobiology* 29: 480–491.

Ubukata, T. 2004. A three-dimensional digitizing system based on triangulation using multiple viewing images [in Japanese, with English abstract]. *Geoscience Reports of Shizuoka University* 31: 65–72.

Ubukata, T. 2005. Theoretical morphology of bivalve shell sculptures. *Paleobiology* 31: 643–655.

Ward, P. 1980. Comparative shell shape distribution in Jurassic–Cretaceous ammonites and Jurassic–Tertiary nautilids. *Paleobiology* 6: 32–43.

Westerman, G.E.G. 1966. Covariation and taxonomy of the Jurassic ammonite *Sonninia adicra* (Waagen). *Neues Jahrbuch für Geologie und Paläontologie, Abhandlungen* 124: 289–312.

Yacobucci, M.M. 2004. Buckman's Paradox: variability and constraints on ammonoid ornament and shell shape. *Lethaia* 37: 57–69.

http://app.pan.pl/acta53/app53-113.pdf

Appendix 1

Specimens examined and measured values of parameters. All specimens have the prefix UMUT. The higher taxonomy follows Korn and Klug (2002) for Devonian ammonoids, Bogoslovskaya et al. (1999) for Carboniferous and Perminan ammonoids, and Page (1996) for Mesozoic ammonoids.

Order	Family	Species	a_e	a_r	S	W_c	D	$A^{0.5}/L$	Specimens	Age	Locality
Agoniatitida	Latanarcestidae	*Latanarcestes* sp.	1.01	1.14	1.22	1.55	0.21	0.17	PM-29049	Devonian	Taouz, Morocco
	Agoniatitidae	*Fidelites* sp.	1.06	1.06	0.75	2.60	0.18	0.24	PM-29050	Devonian	Erfoud, Morocco
		Achguigites sp.	1.12	0.83	0.66	2.29	0.12	0.21	PM-29051	Devonian	Erfoud, Morocco
	Ponticeratidae	*Pseudoprobeloceras costulatum*	1.09	0.96	0.82	1.98	0.31	0.23	PM-29052	Devonian	Taouz, Morocco
	Beloceratidae	*Beloceras* sp.	1.11	0.97	0.30	2.36	0.16	0.16	PM-29053	Devonian	Erfoud, Morocco
	Anarcestidae	*Anarcestes mateviai*	1.04	0.98	0.91	3.08	0.21	0.23	PM-29054	Devonian	Erfoud, Morocco
	Werneroceratidae	*Praewerneroceras hollardi*	1.00	1.10	1.62	1.94	0.38	0.21	PM-29055	Devonian	Taouz, Morocco
	Cabrieroceratidae	*Cabrieroceras* sp.	0.95	1.14	2.79	1.40	0.53	0.19	PM-29056	Devonian	Taouz, Morocco
	Sobolewiidae	*Subanarcestes* sp.	0.99	1.03	1.63	1.46	0.25	0.19	PM-29057	Devonian	Erfoud, Morocco
	Pharciceratidae	*Stenopharciceras viseireuge*	1.04	1.17	0.82	1.95	0.13	0.19	PM-29058	Devonian	Taouz, Morocco
Goniatitida	Tornoceratidae	*Tornoceras* sp.	1.03	1.01	0.77	1.86	0.03	0.17	PM-29059	Devonian	Fezzou, Morocco
		Epitornoceras mithracoides	0.98	1.14	0.69	1.76	0.00	0.16	PM-29060	Devonian	Taouz, Morocco
	Pseudoclymeniidae	*Pseudoclymenia dillensis*	1.04	0.91	0.79	1.84	0.40	0.22	PM-29061	Devonian	Aktyubinsk, Kazakhstan
	Cheiloceratidae	*Cheiloceras uncIulosum*	0.96	1.11	1.23	1.82	0.03	0.18	PM-29062	Devonian	Taouz, Morocco
	Sporadoceratidae	*Sporadoceras* sp. 1	0.98	1.17	1.03	1.70	0.01	0.16	PM-29063	Devonian	Taouz, Morocco
		Sporadoceras sp. 2	1.06	1.05	1.00	2.29	0.02	0.13	PM-29064	Devonian	Taouz, Morocco
		Sporadoceras muensteri	1.01	1.16	0.78	1.89	0.00	0.15	PM-29065	Devonian	Aktyubinsk, Kazsakhstan
	Prolobitidae	*Prolobites delphinus*	0.96	1.16	1.68	1.49	0.21	0.17	PM-29066	Devonian	Aktyubinsk, Kazakhstan
	Pseudohaloritidae	*Neoaganides* sp.	1.10	0.91	0.98	2.28	0.05	0.20	PM-29067	Carboniferous	Texas
	Girtyoceratidae	*Girtyoceras meslerianum*	1.10	1.01	0.79	2.44	0.18	0.19	PM-29068	Carboniferous	Jackforth Creek, Oklahoma
	Goniatitidae	*Goniatites* aff. *crenestria*	0.99	1.02	1.42	1.60	0.05	0.18	PM-29069	Carboniferous	Jackforth Creek, Oklahoma
		Goniatites multiliratus	1.02	0.99	1.18	1.90	0.04	0.18	PM-29070	Carboniferous	Jackforth Creek, Oklahoma
			0.98	1.02	1.30	2.08	0.04	0.19	PM-29071		
	Glaphyritidae	*Glaphyrites hyattianus*	0.99	1.23	1.54	1.92	0.32	0.21	PM-29072	Carboniferous	Oklahoma
		Glaphyrites clinei	1.05	0.95	1.89	1.72	0.31	0.21	PM-29073	Carboniferous	Oklahoma
			1.03	1.01	1.71	1.86	0.31	0.21	PM-29074		
	Reticuloceratidae	*Retites semiretia*	1.04	1.05	2.04	1.67	0.35	0.20	PM-29075	Carboniferous	Thompson Co., Arkansas
	Bisatoceratidae	*Bisatoceras* sp.	1.00	1.03	1.35	1.72	0.20	0.20	PM-29076	Carboniferous	Oklahoma
			1.06	0.97	1.33	1.87	0.11	0.20	PM-29077		
	Thalassoceratidae	*Thalassoceras gemmellaroi*	1.03	1.06	0.87	2.39	0.01	0.19	PM-29078	Permian	Actasty R., S. Ural, Kazakhstan
	Adrianitidae	*Crimites subkrotovi*	0.95	1.08	1.52	1.54	0.04	0.19	PM-29079	Permian	Actasty R., S. Ural, Kazakhstan
	Vidrioceratidae	*Peritrochia typicus*	0.99	1.04	1.20	1.92	0.08	0.19	PM-29080	Permian	Actasty R., S. Ural, Kazakhstan
			0.90	1.08	1.29	1.99	0.07	0.19	PM-29081		
		Peritrochia invaribilis	0.98	1.05	1.39	1.62	0.06	0.17	PM-29082	Permian	Actasty R., S. Ural, Kazakhstan
	Neostacheoceratidae	*Stacheoceras undatus*	1.09	0.88	0.77	2.48	0.24	0.23	PM-29083	Permian	Mangyskhav, Russia
	Paragastrioceratidae	*Paragastrioceras* sp.	1.06	0.96	0.85	2.26	0.32	0.24	PM-29084	Permian	Actasty R., S. Ural, Kazakhstan
		Uraloceras involutum	1.02	1.01	1.39	1.59	0.46	0.23	PM-29085	Permian	Actasty R., S. Ural, Kazakhstan
	Metalegoceratidae	*Metalegoceras* sp.	0.98	1.14	2.71	1.39	0.56	0.20	PM-29086	Permian	Actasty R., S. Ural, Kazakhstan
	Eothinitidae	*Eothinites kargalensis*	1.10	1.04	1.31	1.55	0.59	0.24	PM-29087	Permian	Actasty R., S. Ural, Kazakhstan
	Popanoceratidae	*Popanoceras annae*	1.04	1.08	0.79	1.91	0.10	0.17	PM-29088	Permian	Actasty R., S. Ural, Kazakhstan
Clymeniida	Cymaclymeniidae	*Cymaclymenia* sp. 1	1.06	1.01	0.76	2.40	0.22	0.21	PM-29089	Devonian	Morocco
		Cymaclymenia sp. 2	1.03	0.92	0.74	1.92	0.25	0.24	PM-29090	Devonian	Morocco
	Platyclymeniidae	*Platyclymenia* sp. 1	1.25	0.96	0.78	1.96	0.44	0.26	PM-29091	Devonian	Morocco
		Platyclymenia sp. 2	1.16	1.13	0.82	1.76	0.40	0.25	PM-29092	Devonian	Morocco
		Platyclymenia pompeckyi	1.03	0.96	0.90	1.82	0.37	0.24	PM-29093	Devonian	Aktyubinsk, Kazakhstan
	Clymeniidae	*Oxyclymenia* sp.	0.98	0.85	0.80	1.59	0.54	0.26	PM-29094	Devonian	Morocco
	Wocklumeriidae	*Wocklumeria sphaeroides*	0.95	1.18	1.93	1.23	0.26	0.17	PM-29095	Devonian	Wocklum, Germany

Order	Family	Species	a_e	a_r	S	W_c	D	$A^{0.5}/L$	Specimens	Age	Locality
Prolecanitida	Daraelitidae	*Boesites* sp.	1.11	1.04	0.89	1.99	0.30	0.25	PM-29096	Carboniferous	Rochelle, Texas
		Daraelites elegans	1.11	0.89	0.68	2.77	0.22	0.23	PM-29097	Permian	Actasty R., S. Ural, Kazakhstan
	Propinacoceratidae	*Akmilleria electraensis*	1.13	1.06	0.39	2.52	0.06	0.17	PM-29098	Permian	White Pine Country, Nevada
	Medliocottiidae	*Medlicottia intermedia*	1.13	1.15	0.35	2.79	0.05	0.17	PM-29099	Permian	Actasty R., S. Ural, Kazakhstan
	Pronoritidae	*Neopronorites skvorzovi*	1.03	1.01	0.72	2.79	0.13	0.21	PM-29100	Permian	Actasty R., S. Ural, Kazakhstan
Ceratitida	Xenodiscidae	*Xenoceltites youngi*	1.05	0.97	0.60	1.97	0.29	0.22	MM-29102	Triassic	Crittenden Spring, Nevada
		Xenoceltites subevolutus	0.94	0.81	0.83	1.88	0.50	0.26	MM-29103	Triassic	Spitsbergen, Norway
	Paraceltitidae	*Paraceltites elegans*	0.97	0.61	0.62	1.66	0.51	0.26	PM-29101	Permian	Gaudalupe Mts., Texas
	Sageceratidae	*Pseudosageceras* sp.	0.97	1.19	0.31	2.69	0.00	0.14	MM-29104	Triassic	Spitsbergen, Norway
	Paranannitidae	*Paranannites aspenensis*	1.00	1.07	1.04	1.89	0.19	0.19	MM-29105	Triassic	Crittenden Spring, Nevada
		Paranannites spathi	0.92	1.34	2.16	1.50	0.29	0.17	MM-29106	Triassic	Crittenden Spring, Nevada
		Paranannites sp.	1.01	1.13	1.34	1.76	0.24	0.20	MM-29107	Triassic	Crittenden Spring, Nevada
	Melagathiceratidae	*Arnautoceltites septentrionalis*	1.00	1.15	1.26	1.60	0.23	0.20	MM-29108	Triassic	Crittenden Spring, Nevada
	Arcestidae	*Proarcestes gabbi*	0.97	1.25	1.17	1.65	0.04	0.17	MM-29109	Triassic	West Humboldt Range, Nevada
	Ptychitidae	*Nevadisculites* sp.	0.95	1.13	1.88	1.01	0.05	0.15	MM-29110	Triassic	Favret Canyon, Nevada
	Meekoceratidae	*Meekoceras gracilitatis*	1.03	0.96	0.64	2.50	0.19	0.21	MM-29111	Triassic	Crittenden Spring, Nevada
		Dieneroceras spathi	0.95	1.14	0.59	2.07	0.39	0.23	MM-29112	Triassic	Crittenden Spring, Nevada
		Arctoceras blomstrandi	1.10	1.28	0.81	2.02	0.26	0.22	MM-29113	Triassic	Spitsbergen, Norway
	Ceratitidae	*Paraceratites cricki*	1.09	0.78	0.68	1.90	0.28	0.23	MM-29114	Triassic	South Tobin Range, Nevada
	Beyrichitidae	*Frechites* sp.	1.07	0.93	1.17	1.97	0.35	0.25	MM-29115	Triassic	West Humboldt Range, Nevada
	Proteusitidae	*Tropigastrites lahontanus*	1.09	0.96	1.31	1.47	0.52	0.25	MM-29116	Triassic	South Tobin Range, Nevada
		Favreticeras wallacei	1.09	0.90	0.52	2.21	0.13	0.19	MM-29117	Triassic	McCoy Mine, Nevada
	Proteusitidae	*Tropigastritis louderbacki*	1.00	0.84	0.86	1.54	0.52	0.24	MM-29118	Triassic	West Humboldt Range, Nevada
		Stolleyites tenuis	1.00	1.10	0.45	1.65	0.00	0.13	MM-29119	Triassic	Spitsbergen, Norway
	Tropitidae	*Pleurotropites* sp.	0.97	1.12	1.33	1.93	0.04	0.20	MM-29120	Triassic	Block Mts., California
Ammonitida	Phylloceratidae	*Phylloceras consanguineum*	1.06	1.02	0.52	2.47	0.09	0.19	MM-29121	Jurassic	Sakaraha, Madagascar
		Phylloceras sp.	1.04	1.06	0.64	2.41	0.07	0.19	MM-29122	Cretaceous	Mahajang, Madagascar
		Holcophylloceras sp.	1.09	0.96	0.64	2.18	0.15	0.20	MM-29123	Jurassic	Sakaraha, Madagascar
		Calliphylloceras sp.	1.04	1.00	0.66	1.74	0.13	0.18	MM-29124	Jurassic	Sakaraha, Madagascar
		Ptychophylloceras sp.	1.04	1.01	0.78	2.33	0.04	0.20	MM-29125	Jurassic	Sakaraha, Madagascar
		Phyllopachyceras ezoense	1.08	1.00	0.98	2.94	0.03	0.21	MM-29126	Cretaceous	Saku, Hokkaido, Japan
			1.04	0.96	1.00	2.61	0.01	0.20	MM-29127		
		Hypophylloceras subramosum	1.08	0.94	0.62	2.81	0.07	0.20	MM-29128	Cretaceous	Kotanbetsu, Hokkaido, Japan
	Ussuritidae	*Indigirophyllites spetsbergensis*	1.06	0.84	0.77	2.47	0.26	0.25	MM-29129	Triassic	Spitsbergen, Norway
	Juraphyllitidae	*Tragophylloceras ibex*	0.95	1.01	0.47	1.62	0.24	0.20	MM-29130	Jurassic	Osuabrük, Germany
	Lytoceratidae	*Pterolytoceras* sp.	1.07	0.72	1.03	2.17	0.42	0.28	MM-29131	Jurassic	Sakaraha, Madagascar
		Argonauticeras sp.	1.08	0.79	1.16	1.99	0.41	0.28	MM-29132	Cretaceous	Mahajang, Madagascar
	Tetragonitidae	*Tetragonites glabrus*	1.07	0.97	1.16	2.14	0.32	0.24	MM-29133	Cretaceous	Tappu, Hokkaido, Japan
			1.08	0.91	1.04	2.72	0.20	0.24	MM-29134		
		Tetragonites popetensis	1.10	0.92	0.83	1.86	0.30	0.23	MM-29135	Cretaceous	Saku, Hokkaido, Japan
		Eotetragonites sp.	1.04	0.93	1.31	1.86	0.46	0.25	MM-29136	Cretaceous	Mahajang, Madagascar
	Gaudryceratidae	*Gaudryceras striatum*	1.07	0.94	1.03	1.99	0.33	0.24	MM-29137	Cretaceous	Saku, Hokkaido, Japan
		Gaudryceras tenuiliratum	1.03	1.00	1.23	1.87	0.44	0.25	MM-29138	Cretaceous	Saku, Hokkaido, Japan
		Gaudryceras denseplicatum	1.10	0.87	0.87	2.22	0.26	0.25	MM-29139	Cretaceous	Tappu, Hokkaido, Japan
		Anagaudryceras limatum	0.92	1.12	1.04	2.01	0.32	0.25	MM-29140	Cretaceous	Kotanbetsu, Hokkaido, Japan
	Scaphitidae	*Yezoites planus*	1.02	1.02	1.27	2.73	0.30	0.24	MM-29141	Cretaceous	Tappu, Hokkaido, Japan
	Douvilleiceratidae	*Douvilleiceras* sp.	1.05	0.88	0.91	2.20	0.37	0.26	MM-29142	Cretaceous	Mahajang, Madagascar
		Hypacanthoplites subcornuerianus	1.07	0.80	1.48	2.31	0.32	0.26	MM-29143	Cretaceous	Miyako, Iwate, Japan
	Psiloceratidae	*Psiloceras pacificum*	0.97	0.91	0.84	1.93	0.39	0.24	MM-29144	Jurassic	New York Canyon, Nevada
	Arietitidae	*Agassiceras sciplonianum*	1.06	0.71	1.21	2.09	0.47	0.26	MM-29145	Jurassic	Salzgitter, German
	Hildoceratidae	*Harpoceras exavatum*	1.07	1.00	0.59	2.16	0.23	0.22	MM-29146	Jurassic	Lünde Kanal, Germany
		Grammoceras doerntense	1.26	1.00	0.66	1.75	0.24	0.22	MM-29147	Jurassic	Döruten, Germany
	Graphoceratidae	*Leioceras opalinum*	1.15	0.83	0.54	2.23	0.22	0.21	MM-29148	Jurassic	Göppingen, Germany

Order	Family	Species	a_e	a_r	S	W_c	D	$A^{0.5}/L$	Specimens	Age	Locality
Ammonitida	Oppeliidae	*Taramelliceras* sp.	1.03	0.95	0.52	2.73	0.09	0.20	MM-29149	Jurassic	Sakaraha, Madagascar
		Lissoceras sp.	1.02	0.90	0.69	2.62	0.26	0.24	MM-29150	Jurassic	Sakaraha, Madagascar
	Perisphinctidae	*Kranaosphinctes* sp.	0.95	0.87	1.08	2.02	0.49	0.26	MM-29151	Jurassic	Sakaraha, Madagascar
		Grossouvia sp.	1.02	0.81	0.82	2.21	0.41	0.26	MM-29152	Jurassic	Sakaraha, Madagascar
	Aspidoceratidae	*Aspidoceras* sp.	1.03	0.92	1.48	2.09	0.28	0.24	MM-29153	Jurassic	Sakaraha, Madagascar
		Euaspidoceras sp.	0.99	0.61	0.77	2.70	0.37	0.27	MM-29154	Jurassic	Sakaraha, Madagascar
	Craspeditidae	*Craspedites subditus*	1.03	1.10	1.10	1.68	0.28	0.19	MM-29155	Jurassic	Volga River, Russia
	Desmoceratidae	*Desmoceras* sp.	0.99	0.99	1.15	2.22	0.20	0.22	MM-29156	Cretaceous	Mahajang, Madagascar
		Tragodesmoceroides subcostatus	1.04	0.98	0.91	2.23	0.11	0.20	MM-29157	Cretaceous	Tappu, Hokkaido, Japan
		Damesites sugata	1.03	1.02	0.85	1.99	0.09	0.19	MM-29158	Cretaceous	Saku, Hokkaido, Japan
		Damesites semicostatus	1.04	0.96	0.90	2.37	0.07	0.21	MM-29159	Cretaceous	Tappu, Hokkaido, Japan
		Damesites sp.	1.07	0.98	0.86	2.05	0.12	0.20	MM-29160	Cretaceous	Saku, Hokkaido, Japan
		Hauericeras angustum	1.06	0.73	0.68	2.41	0.40	0.24	MM-29161	Cretaceous	Saku, Hokkaido, Japan
	Puzosidae	*Puzosia* sp.	1.01	0.98	1.14	2.13	0.36	0.25	MM-29162	Cretaceous	Mahajang, Madagascar
	Silesitidae	*Neosilesites* sp.	0.96	0.70	0.82	1.94	0.47	0.25	MM-29163	Cretaceous	Mahajang, Madagascar
	Kossmaticeratidae	*Yokoyamaoceras ishikawai*	1.15	0.78	0.84	2.33	0.32	0.23	MM-29164	Cretaceous	Saku, Hokkaido, Japan
			1.05	0.97	0.82	1.91	0.33	0.24	MM-29165		
			1.00	0.89	0.90	1.99	0.34	0.23	MM-29166		
	Cleoniceratidae	*Cleoniceras* sp.	1.00	0.97	0.62	2.62	0.20	0.21	MM-29167	Cretaceous	Mahajang, Madagascar
	Pachydisidae	*Anapachydiscus naumanni*	1.05	0.92	1.40	2.09	0.24	0.23	MM-29168	Cretaceous	Saku, Hokkaido, Japan
		Teshioites ryugasensis	1.02	0.95	0.91	2.08	0.25	0.22	MM-29169	Cretaceous	Saku, Hokkaido, Japan
		Canadoceras kosmatti	1.00	1.00	1.14	2.13	0.27	0.23	MM-29170	Cretaceous	Saku, Hokkaido, Japan
	Hoplitidae	*Neogastroplites meulleri*	1.04	0.98	0.66	2.65	0.13	0.21	MM-29171	Cretaceous	Petroleum Country, Montana